35th AIAA Fluid Dynamics Conference and 36th AIAA Plasma Dynamics and Lasers Conference
6-9 June 2005, Toronto, Canada

Multidimensional Collisional Dielectric Barrier Discharge for Flow Separation Control at Atmospheric Pressures

Subrata Roy*
Computational Plasma Dynamics Laboratory, Kettering University, Flint, MI 48504, USA

and

Datta V. Gaitonde†
Computational Sciences Branch, Air Force Research Laboratory, Wright Pat AFB, Ohio 45433, USA

Radio frequency based discharges at atmospheric pressures are the focus of increased interest in aerodynamics because of a wide range of potential applications including specifically actuation in flows at moderate speeds. Recent literature describing promising experimental observations, especially on separation control, have spurred efforts in the development of parallel theoretical modeling to alleviate limitations in current understanding of the actuation mechanism. The present effort builds on a recently developed finite element-based one- and two-dimensional multi-fluid formulation of plasma–sheath for atmospheric optical glow discharge in partially ionized gas. The model was relatively straightforward but formed the foundation of a versatile first-principles based methodology. Higher-fidelity models are included to yield a more sophisticated framework to predict discharge-induced momentum exchange. Here, the complete problem of a dielectric barrier discharge based separation control with axially displaced electrodes is simulated in a self-consistent manner. Model predictions for transient evolution of charge densities, the electric field, electrodynamic force and induced gas velocity distributions for helium gas in quiescent condition are shown to mimic trends reported in the experimental literature. For the first time, results also document the decay process of a separation bubble formed due to flow past a flat plat inclined at 12 deg angle of attack. This effort sets the basis for extending the formulation further to include polyphase power input in multi-dimensional settings, and to apply the simulation method to flows past common aerodynamic configurations.

Nomenclature

A,B	Coefficients
C	Capacitance, farad
D	Diffusion coefficient, cm^2/s
d	Characteristic length, cm
E	Electric field, V/cm
e	Electron charge, coulomb
ε	Permittivity, farad/m
F	Solution residual
ϕ	Potential, V
Γ	Flux, cm^{-2}/s
I	Current, Amp/cm^2
λ_{De}	Electron Debye length, χm
λ_i	Ion mean free path, cm
m	mass, kg
μ	Mobility, $cm^2V^{-1}s^{-1}$
n	Number density, cm^{-3}
ω	Applied frequency, radians
Ω	Computational domain

* Associate Professor of Mechanical Engineering, 1700 West Third Avenue, and AIAA Associate Fellow.
† Technical Area Leader, Air Vehicles Directorate/VAAC, 2210 8th St., and AIAA Associate Fellow.

p Pressure, torr
r Recombination coefficient
T Temperature, eV
t Time coordinate, s
V Species velocity, m/s
x Spatial coordinate, cm
z ionization rate, /s

Subscripts:
α Species
B Bohm
e Electron, finite element
f fluid
i Ion
n neutral
0 Reference value

I. Introduction

RECENT research efforts[1-7] have demonstrated the feasibility of utilizing dielectric barrier discharges (DBDs) to improve the lift-drag characteristics and inhibit phenomena such as stall on airfoils. A particularly attractive feature of these plasma-based devices is their capacity to operate at atmospheric conditions, without uncontrolled macroscopic breakdown. Experimental efforts[1-3] have identified many of the key parameters, most prominent among which are the geometric configuration and the form of the applied excitation. Specifically, the embedded electrode is displaced in the streamwise direction relative to the exposed electrode which lies on the surface of the object, such as the airfoil. The asymmetry in the location of the electrodes, coupled with the phase shift of the electrode when multiple devices are present, yields a directional asymptotic "push" on the bulk gas.

A typical schematic of such actuators is shown in Figure 1. The electrode arrangement is such that the insulator surrounds the grounded electrode and a voltage powered at radio frequency (rf) is applied to the electrode exposed to the gas. In another arrangement, both electrodes are powered separated by a beat frequency. A complex unsteady interaction occurs between the two electrodes, details of which depend on frequency, voltage, geometric configuration and dielectric constants of the media. Experimental evidence shows that there is no runaway state for the parameters under consideration and that an asymptotic (quasi) periodic state is reached, with a dominant frequency that is similar to the input perturbation. For a given inter-electrode distance, as the applied voltage becomes sufficiently large, the dielectric surface adjacent to the rf electrode produces a barrier discharge, which weakly ionizes the surrounding gas. The combination of electrodynamic body force and collisional processes whose detailed mechanics is yet to be understood, ultimately transfers momentum acquired from the electric field by the charged particles to the neutrals which are the primary species.

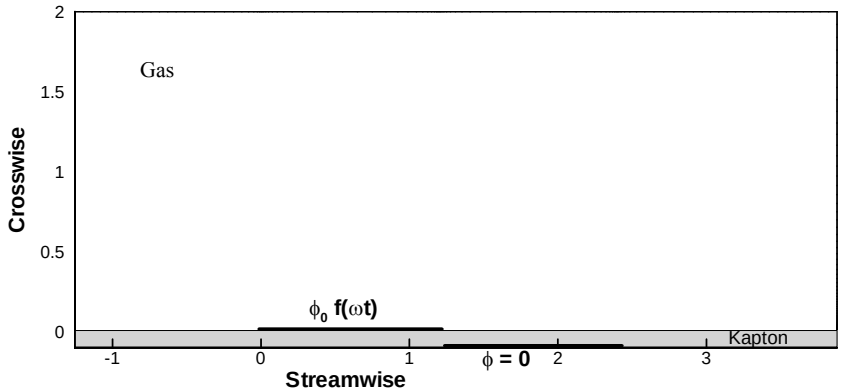

Figure 1. Schematic of the RF induced dielectric barrier discharge device. The shaded region is an insulator with embedded (grounded, $\phi = 0$) and exposed (powered, ϕ_0 f(ωt)) electrodes shown in thick solid line segments.

Benefits of these actuators include precise application of large electrodynamic body forces, active control of these forces, and their striking effects on the flow. These capabilities added with the absence of any moving components make these actuators very useful for flow control in wall layers or separated layers at both low[1-7] and high speeds.[8,9] The parameters employed in experimental observations include peak-to-peak voltage between 2-20 kV at 1-50 kHz rf, which are suitable for actuation at atmospheric pressure at low speeds to *O*(10) torr at high-speeds. Specifically at high

pressures, the fluid is highly collisional, inducing an efficient momentum transfer between charged and neutral species. The collisional rf sheath dynamics of near-surface regions are fundamentally different than that under direct current (*dc*) and/or collisionless conditions and substantially more difficult to simulate because of their unsteady nature. While dc-based methods are a useful study for energy interactions of an already ionized flow, recent literature[8-10] shows that energy budgets will depend crucially on dynamic non-equilibrium ionization techniques. The load factor for dc sheath application is of order 1, far from the most energy efficient Stoletow point, thus generally unsuitable for ionization purposes. The experimental successes of rf induced dielectric barrier discharge (DBD) using air at atmospheric condition[1,3] thus ushers tremendous interest in the electrogasdynamic flow control and energy management community. Microfilaments of nanosecond duration with many current pulses in a half cycle maintain the optical glow in DBD. The small time scale of the discharge limits charge transport and allows minimal heating of the bulk gas.[6,11] Thus most of the electric energy is utilized for exciting the carrier gas resulting in efficient applications to boundary layer flow actuation.

This paper focuses on modeling the physics of a plasma actuator, shown in Figure 1, about which a surface barrier discharge controls the surrounding neutral gas flow. Several configurations have been proposed and tested to exploit the complex interaction between the electric field and the fluid around such actuators. A detailed discussion may be found in Ref. 1,3.

While experimental efforts on atmospheric DBD interactions for flow actuation are ample and extensive, the theoretical modeling effort that span a range of phenomenological to rudimentary first principle based methods[2,4-7,12] is yet to explain the underlying physics. Roth[3] postulated a balance between the electrostatic force and the hydrodynamic force to estimate the induced gas velocity. Enloe et al.[2] analytically showed that this postulation only holds for a simple one-dimensional configuration and demonstrated the need for two dimensional electric force modeling for understanding the DBD flow actuation process. Based on experimental observation, Shyy et al.[4] assumed a triangular distribution of the electrostatic body force downstream of the electrode with a constant charge density and then utilized the Navier-Stokes equation to predict its effects on the flow. Recently, Gaitonde et al.[12] have described the response of the flow past a stalled NACA 0015 airfoil at 15 deg angle of attack to phenomenological approximate body forces originating from asymmetric dielectric-barrier-discharge actuators using direct numerical simulations.

For accuracy and fidelity, however, it is imperative that the force model be derived from first principles through a simulation of the elementary mechanisms that yield the discharge characteristics and flow actuation similar to that found in the experiments. Roy and Gaitonde demonstrated such a model, first for volume discharge between two dielectric coated electrodes[5] and then for capturing effects of surface discharge on quiescent helium gas[6,7], using a finite element-based multi-dimensional multi-fluid formulation of plasma–sheath at atmospheric conditions. While the first model was relatively basic, the two dimensional model of collisional surface dielectric barrier discharge documented a consistent first principles formulation of charge and neutral number densities, their momentum dynamics, electrostatic field and potential distribution for an asymmetric DBD configuration. The model treated the insulator and the gas simultaneously and integrated the Poisson equation into the charge and gas dynamics. The study was focused on understanding the effects of symmetric and asymmetric electrode arrangements. Simulation results for asymmetric arrangement from Ref. 6 as shown in Figure 2 compared qualitatively with reported rf discharges[1-3] in partially ionized helium gas.

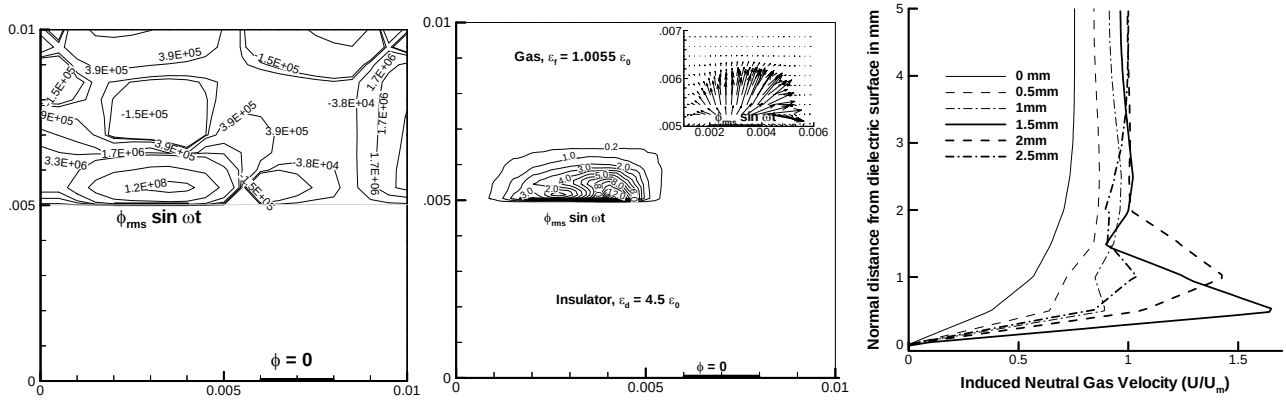

Figure 2. Plasma actuation of quiescent helium gas.[6] (a) Charge particle distribution, (b) force variation about the electrode-dielectric surface, (c) streamwise gas velocity profiles at different locations along the flow.

As a logical extension of our previous work, the goal of the present effort is to implement the developed two-dimensional model to practical single electrode-pair systems for understanding the response of body force characteristics resulting from the collisional surface discharge to separated gas flows at atmospheric pressures. An efficient, robust, module-based multiscale ionized gas (MIG) flow finite-element code suitable for accurate imposition of complicated boundary conditions is employed. The body force is computed self-consistently from the three-body electro gas

dynamics using the applied rf potential and the dielectric properties of insulator and gas media based on first principles. For simplicity, here again helium is used as the carrier gas because of its relative stability in maintaining the discharge optical glow (as compared to air, nitrogen, oxygen and argon which transition into an unstable filamentary discharge for the same electrode gap and pressure[11]). Note the model is easily extendible to complex configurations and more accurate transport properties when they become available from ongoing experimental efforts being performed elsewhere. Two simulations, one with quiescent gas, the other with an imposed upstream gas velocity are documented here showing not only plasma events but also the evolution of separated flow control about an actuator.

This paper is organized as follows. Section II describes the problem statement. Section III specifies the boundary conditions. Section IV explains the methodology used to solve the system of equations. Section V describes and interprets the computed results. Section VI summarizes the conclusions.

II. Problem Statement

Assuming only positive ions, negative electrons and neutral particles, the following two-dimensional three-body collisional plasma-sheath model is solved.

Charge continuity: $$\frac{\partial n_\alpha}{\partial t} + \frac{\partial n_\alpha V_{\alpha j}}{\partial x_j} = n_e z - r n_e n_i \qquad (1a)$$

Charge momentum: $$n_\alpha V_{\alpha j} = -\mathrm{sgn}(e) n_\alpha \mu_\alpha \frac{\partial \phi}{\partial x_j} - D_\alpha \frac{\partial n_\alpha}{\partial x_j} \qquad (1b)$$

Potential: $$\varepsilon\left(\frac{\partial^2 \phi}{\partial x_j^2}\right) = e(n_e - n_i) \qquad (2)$$

Neutral continuity: $$\frac{\partial n_n}{\partial t} + \frac{\partial n_n V_{nj}}{\partial x_j} = -n_e z + r n_e n_i \qquad (3)$$

The charge particle $\alpha = e,i$ distributions are considered non-Maxwellian. The electron temperature is nearly uniform at 1eV = 11,600K and the ions and neutrals are in local thermal equilibrium at 300K. The working gas helium is maintained at 300 torr bulk pressure at 300K. For the operating condition of interest, the inertia terms are small relative to the effect of the electrostatic field and collisional interactions, and thus neglected. The collisional momentum exchange is vital to the charge-to-neutral momentum transfer.

The electron diffusion is obtained from Einstein relation, $D_e = (T_e / e)\mu_e$, where T_e is the energy in electron volts, e is the elementary charge, ε is the permittivity, and $\mu_e = e/(m_e \nu_{eh})$ is mobility of an electron, where $\nu_{en} \approx 10^{12}$/s is the electron-neutral collision frequency. In this context, we note that transport properties, which have been taken from the literature, are to be viewed as nominal values facilitating the development of the numerical framework, rather than to fill gaps in current thermo-chemical data for the environment of interest. In this same vein, D_i is the ion diffusion[14] in cm^2/s at 300K, and the ion mobility μ_i is given as an empirical relation that contains the electric field and pressure, assuring consideration of collisional effects.[7,14] However, quantitative results will depend on the nominally chosen values. The ionization rate z for the working gas is $z^i/n_n = \langle V_e \sigma^i(V_e) \rangle$, the averaging is done over the velocities of the electrons whose energy is sufficient for ionization $mV_e^2/2 > H_i$, the first ionization potential. Here z is based on the Townsend first ionization.[6,7] The ionization process can be described as $e + He \rightarrow He^+ + e + e'$ where e and e' have different energy levels. Processes like $He \rightarrow He^{++}$ and $He^+ \rightarrow He^{++}$ may also play an important role for high voltages, but are not considered here. The coefficient of recombination is given as, $r = \left\langle V_{\mathrm{eth}} \sigma_{ei}^r (V_{\mathrm{eth}}) \right\rangle = 1.09 \times 10^{-14} T^{-9/2} n_e \ \mathrm{cm}^3/\mathrm{s}$. Here, V_{eth} is the electron thermal velocity and σ_{ei} is the electron-ion collision cross-section. For simplicity, we have assumed no secondary electron emission.

Here, the electron plasma frequency, $\omega_{\mathrm{pe}} = 2e\sqrt{(\pi n_e / m_e)}$, is much higher than the applied voltage frequency. Also, the momentum exchange terms due to electron-electron and ion-ion interaction are negligible in comparison with the electron-ion and ion-neutral momentum exchange as the relative drift between similar particles is small in comparison with the drift between electrons, ions and neutrals.

The dynamics of neutral particles are determined using the following neutral momentum equations:

$$\frac{\partial V_{nj}}{\partial t} + V_{nl} \frac{\partial V_{nj}}{\partial x_l} = \frac{m_e n_e}{m_n n_n} \nu_{en} \left(V_{ej} - V_{nj}\right) + \frac{M n_i}{m_n n_n} \nu_{in} \left(V_{ij} - V_{nj}\right) + n_e z V_{ij} / n_n \qquad (4)$$

The effect of pressure on quiescent neutral flow is assumed negligible. This was chosen for separating the effect of electric field from the pressure field. This assumption is also reasonable for high Reynolds number flows. At this stage, any balance between the electrostatic and fluid dynamic pressure gradients cannot be guaranteed for a fundamentally unsteady process. We use the electrodynamic body force $e(n_i - n_e)\mathbf{E}$ (although no Lorentz force is present,

the force is created by charge transport) to compute the averaged velocity of the fluid is based on the following continuity and momentum equations:

$$\partial\rho/\partial t + \partial\rho V_{fj}/\partial x_j = 0 \tag{5a}$$

$$\frac{\partial V_{fj}}{\partial t} + V_{fl}\frac{\partial V_{fj}}{\partial x_l} = \frac{\varpi}{\rho}e(n_i - n_e)E_j - \frac{RT}{\rho}\frac{\partial \rho}{\partial x_j} + \frac{\partial}{\partial x_l}\tau_{jl}, \tag{5b}$$

where $\tau_{jl} = \frac{\mu}{\rho}\left(\frac{\partial V_{fl}}{\partial x_j} + \frac{\partial V_{fj}}{\partial x_l}\right) - \frac{2}{3}\frac{\mu}{\rho}\frac{\partial V_{fk}}{\partial x_k}\delta_{jl}$ with μ as the gas viscosity (=2.066×10^{-5} Ns/m^2) and δ_{jl} is the Kronecker delta. The factor ϖ is introduced to modulate the effect of electric field. Helium is assumed as an ideal gas.

The multiscale ionized gas (MIG) flow code was used to solve Eqns. (1)-(5). MIG has a module based computational platform that implements the high-fidelity finite-element (FE) procedure adapted from fluid dynamics to overcome the stiffness of the equations generated by multi-species charge separation phenomena. This code has been used and validated for several fluid dynamics[15], ionized gas[5-7,16,17] and micro/nanoscale[18,19] flow problems. FE techniques are especially suitable for their adaptability to arbitrary multidimensional geometries and boundary conditions. Here, a 2D biquadratic FE formulation is employed along with 4th order Runge-Kutta time marching to solve the continuity and momentum equations for all species and fluid. The solution process consists of two steps. First, using Eqns. (1a), (2), (3) and (4), a global matrix is formed and solved simultaneously obviating the need for any special sub-iteration for the Poisson solver. The species density and charge velocity thus calculated are then used in Eqn. (5a-b) to predict the fluid density and velocity. The Galerkin weak statement associated with a variational integral underlines the development of this numerical algorithm. Note that the selection of test function orthogonal to the trial function in Galerkin formulations guarantees the minimization of error[20], making it better suited for these problems. Details of the code are reported elsewhere (for example, see Ref. 15,16). For the species equations (1)-(4), a solution adaptive timescale of upto 100 times the dielectric relaxation timescale[21] is adopted to calculate the charge separation and electric field up to a periodic asymptote. The gas equations (5a-b) are then solved using the volume specific electrodynamic body force to predict the fluid velocity and continuity evolving in time with the flow time scale of ~ms. The solution of the Newton-Raphson iteration is converged at any given timestep when the maximum value of the residual, relative L_2-norm for each of the state variables, becomes smaller than a chosen convergence criterion of 10^{-4}.

III. Boundary Conditions

The two dimensional computational domain (–1.252, 3.880cm)×(-0.1, 2.0cm) consists of a Kapton insulator in the lower half (y: -0.1, 0cm) with a dielectric constant ε_d=3.5 ε_0 and the upper half (y: 0, 2cm) filled with inert helium gas of ε_f = 1.0055 ε_0, where ε_0 is permittivity of vacuum. Inside the insulator the current due to motion of charged particles is forced to zero while the displacement current is balanced with the total current at the gas-dielectric boundary. The schematic in Figure 1 shows two electrodes in which the bottom electrode is grounded and an rf alternating frequency of 5 kHz with rms potential of 1 kV is imposed at the top electrode. Each electrode is infinitesimally thin and 1.2 cm long. They are vertically displaced by 1mm with no horizontal overlap. The highly stretched computational mesh shown in Figure 3 consists of 51 × 53 two-dimensional bi-quadratic Lagrange finite elements. The insulator material is modeled using 12 × 53 biquadratic elements. The nodes are attracted towards the wall and electrode edges for capturing better solution details. The highest and lowest elemental aspect ratios are approximately 90 and 10, respectively.

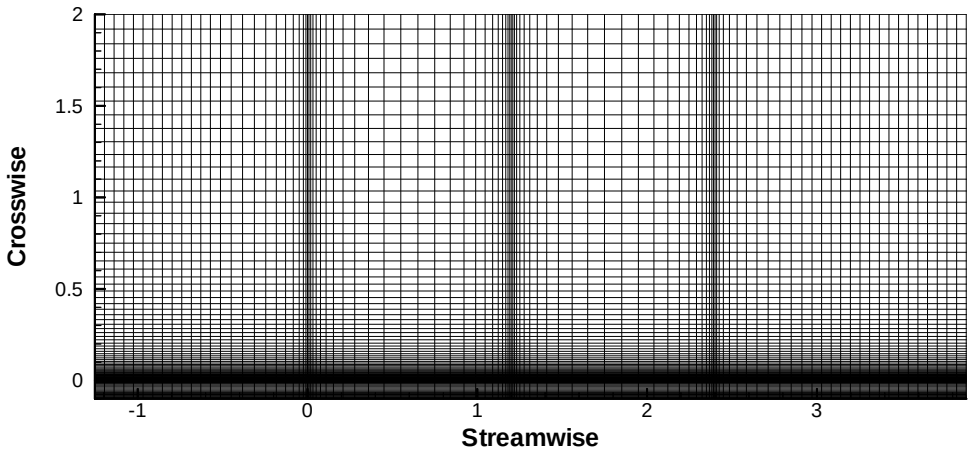

Figure 3. Computational mesh shows highly non uniform nature.

In order to identify the charge characteristics and its effect on gas flow, two different simulations were performed on a single geometric configuration with an asymmetrically displaced electrode-pair arrangement. In the first, no gas velocity was imposed, i.e., quiescent flow. Hereafter, we will denote this as Case A. In the second, an upstream flow of 12 m/s was imposed at $x = -1.252$ cm with an angle of attack (AOA) of +12°. This will be noted as Case B. For all simulations electrons are assumed to be isothermal at the boundary and maintained at 1eV (~11,600K) while the ions are cold (300K) at 300 torr. Zero flux, i.e., homogeneous Neumann boundary conditions are applied at all other boundaries. The solutions are verified by qualitative comparison with the reported results. The results are then employed to explore the enhancement of near wall fluid velocity. No-slip gas velocity boundary condition is imposed for all cases. Also the insulator is considered impermeable to gas.

IV. Methodology

The ionized helium gas is numerically modeled using the finite-element based MIG flow code. The code is modular and separate subroutines can be written to model different physics. Here, the equation sets (1) – (5) can be written with operator L as L (**q**) = 0 ; where **q** contains state variables like densities, velocities and potential. Multiplying with a permissible test function η and integrating over the spatially discretized domain Ω, the variational statement results in the weak form[20]

$$WS^h = \Im_e \left(\int_{\Omega_e} [\eta L(\boldsymbol{q}) d\tau] \right)_e = 0$$

for a discretization h of $\Omega = \bigcup \Omega_e$ and $\Im_e$ is the non-overlapping sum over the elements. Thus, for example, the GWS form of Eq. (2) becomes,

$$\sum_e \left(\int_{\Omega_e} \frac{d\eta}{dz} \frac{d\eta^T}{dz} dz \{\phi\}_e + \int_{\Omega_e} \eta\eta^T dz \{n_e\}_e - \int_{\Omega_e} \eta\eta^T dz \{n_i\}_e - \int_{\Omega_e \cap \partial\Omega_e} \eta \frac{d\eta^T}{dz} dz \{\phi\}_e = F_\phi \right)_e \qquad (6)$$

where F_ϕ is the solution residual.

The Jacobian matrix $J=[\partial F/\partial \boldsymbol{q}]$ in the global $[J].\{\partial \boldsymbol{q}\} = -\{F\}$ is resolved using Generalized Minimal RESidual solver with LU-preconditioner for updating change in discretized solution vector **q** at each iteration. The Newton-Raphson scheme is used to formulate the matrix algebra resulting from nonlinear ordinary differential equation (ODE) systems. The GMRES solver is well suited to handle the sparseness of the resulting stiff matrix. The solution is assumed to have converged at a time-step when the L_2 norm of all solution variables and residual are below a chosen convergence criterion (ε). The convergence criterion for all variables at any iteration is set at 10^{-4}. Solution stability is ensured by appropriate selection of time marching step size and the introduction of artificial diffusion.

V. Results and Discussion

Figures 4 through 11 present computed results for charge densities, electric field lines, current and gas dynamics for simulated cases. Figure 4 displays unsteady evolution of predicted force vectors with electric field lines overlaid on charge density contours (cm^{-3}) for the quiescent Case A. The electric field lines trace the vector path moving in a trajectory from the exposed instantaneous anode to the grounded cathode inside the dielectric in an asymmetric fashion showing a directional bias, first (at π/2 radians, Fig. 4a) towards the right, then towards the left (at π, Fig. 4b and at 3π/2 radians, Fig. 4c), and finally towards the right again at 2π radians (Fig. 4d). The computed results are similar to the experimental data showing that the exposed electrode is situated upstream of the peak location of the electric field and thus the imparted momentum. The dominant acceleration of ions following these lines induces the neutral gas particles through a mechanism entwined with the body force and the ion-neutral collisional momentum transfer. In Fig. 4a, the charge density contours shows a positive peak of 3.4×10^9 cm^{-3} above the embedded electrode (a few Debye length away from the surface) and a negative peak of -1.9×10^9 cm^{-3} on the exposed electrode showing the effects of electric field. The ion density dominates the actuator surface at π radians with a peak of 6.3×10^9 cm^{-3}. At 3π/2, the negative charge (-2.7×10^9 cm^{-3}) accumulates downstream of the exposed electrode and charge density extrema gradually decay as the cycle moves to 2π radians.

The body force calculated based on the product of charge and electric field shows very strong forward and downward moving vectors downstream of the exposed electrode for the positive part of the cycle (see Fig. 4a). At the negative peak of the cycle in Fig. 4c, the force vectors concentrate just upstream of the right edge of the powered electrode with majority forces going backward and downward. However, for the rest of the cycle the force is much smaller as compared to the positive part (~10%, 42% and 2% of the peak magnitude respectively at

π, 3π/2 and 2π radians). The average body force will thus push the bulk gas in the forward and downward direction. Recent numerical simulation[6,7] documented the gas velocity downstream of the right edge of the exposed anode with a two orders of magnitude smaller negative velocity near the left edge of the exposed electrode similar to what we observe here.

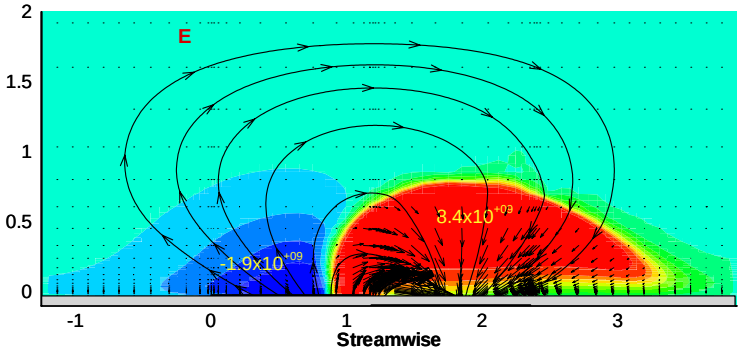

(a) π/2 rad

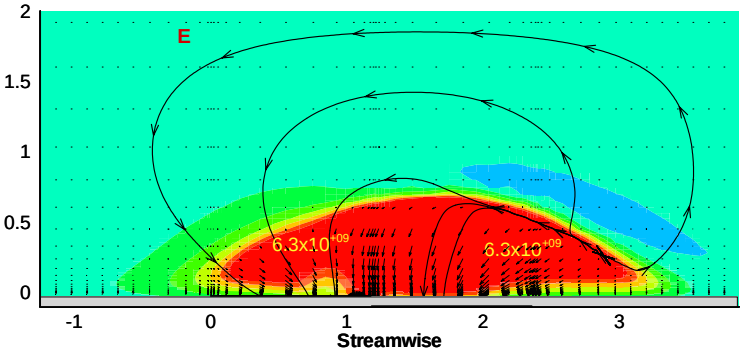

(b) π rad

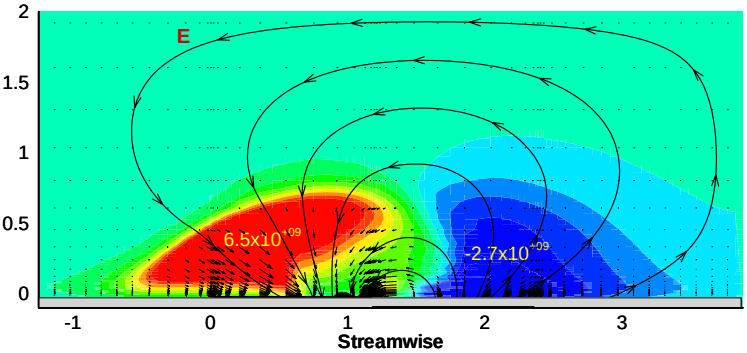

(c) 3π/2 rad

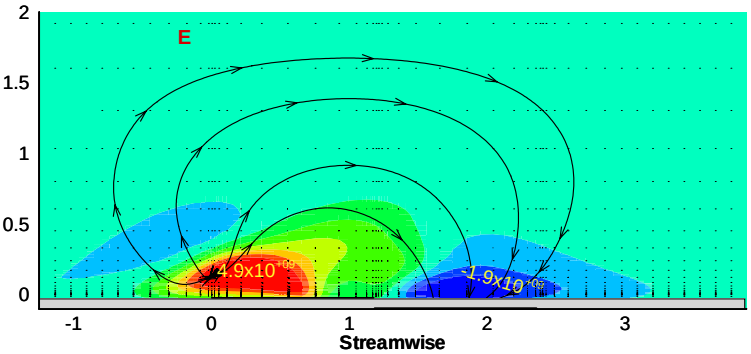

(d) 2π rad

Figure 4. Time evolution of computed electric field lines overlaid on charge density contours (cm^{-3}) with near electrode volume specific force details.

Figure 5 plots the streamwise component of the time average of volume specific body force for Case A. The line trace of the force vectors is showing a directional bifurcation (similar to that reported in a recent PIV experiment[22], Fig. 2) just downstream of the exposed electrode. This will tend to guide the flow in both direction just at about x = 2cm location. The positive peak very close to the dielectric surface is three times higher than the negative peak. Due to fluid inertia, the bulk gas will only respond to this average force which will ensure its net forward motion. The momentum thus imparted to the gas will induce a velocity along the dielectric surface. Figure 6 plots the streamwise component of the gas velocity computed from Eq. (5) for Case A at six local vertical line plots upstream and downstream of the electrode edge and shows a wall jet like feature. The zero flow initial condition makes the computational problem more challenging. The peak of this wall jet of 2.4 m/s occurs at 6 mm downstream of the exposed electrode beyond which diffusive momentum transfer increases the height of the region influenced by the DBD, and the peak velocity diminishes. Similar velocity profiles have been observed by several experimental groups.[1-3,22] Note that for helium gas the mobility is much higher than air and hence the induced velocity is higher.

The peak electron current (not shown) is observed at the two corners (right and left) of the exposed electrode with a peak value of $O10^2$ mA at π radians and the minimum current (two orders of magnitude less than the peak) is computed at $\pi/2$ radians of the phase. An explanation for this behavior may be proposed based on arguments pertaining to the observed self-limiting nature of the discharge. In surface DBD there is no real current path between the electrodes. However, the charge build up on the insulator surface opposes the applied voltage, shutting of the discharge just beyond the peak when the applied voltage starts decreasing, thus self-limiting the system. This is also confirmed by the experimental data (see for example Fig. 2 of Ref. 23) where the current magnitude peaks at about π radians.

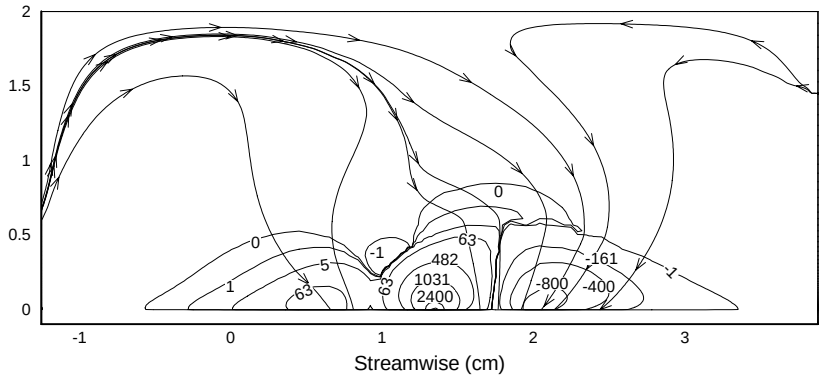

Figure 5. Time average of streamwise component of the μN force per unit volume about the surface of the actuator shows the dominance of the streamwise forward (positive) force component. Line traces show the direction of force which will guide the local flow.

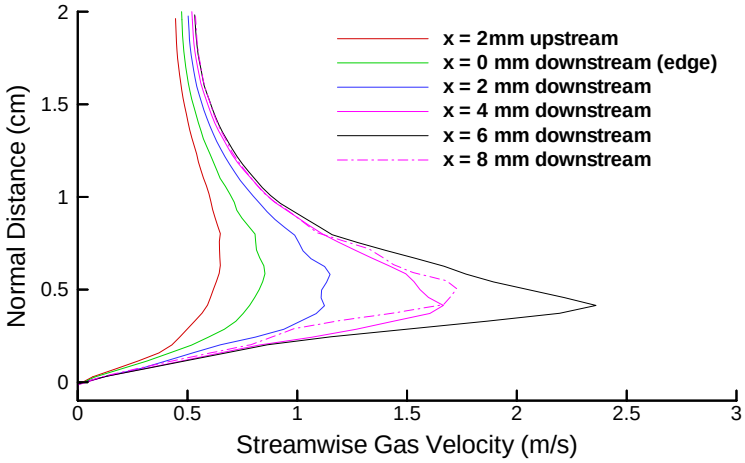

Figure 6. Computed streamwise velocity induced in a quiescent helium gas.

For the actuator model to work for design purposes, it is essential to test it for low speed flow conditions where reasonable amount of supporting experiments have been reported. Figure 7 shows the transient effect of DBD actuator for realistic gas flow control. The timescale of gas flow for the present dimensions is in milliseconds while the plasma timescale is several orders of magnitude less. For this Case B simulation, first an initial flow condition is generated over the flat plate kept at a 12° angle with respect to the helium gas inflow without the rf power turned on. Figure 7a plots the stream traces of gas particles based on the velocity vectors of the initial flow field and shows a strong separated flow (see inset) just downstream of the leading edge of the plate. Then the power is turned on for the same

electrode arrangement as presented earlier. Figures 7b,7c and 7d shows the gradual removal of the recirculation bubble due to the separation as a function of time. The strong positive force contours (in red) shows the time average dynamics of streamwise component as it literally pushes the recirculation off the plate within 6ms. The fluid reacts to the generated mean body force but there may be a slow interaction with the local plasma generation as time progresses. To our knowledge, such description has not been shown in the reported literature to-date. Specific details of gas velocity components and the streamwise force is presented in Figure 8 at five locations along the dielectric at t=6ms. It is interesting to note that the peak force is located at x = 0.7 cm in the middle of the initial bubble while the peak of the wall jet is occurring downstream of the exposed electrode at x = 2.0 cm. The location of the actuator is thus important to control the flow effectively.

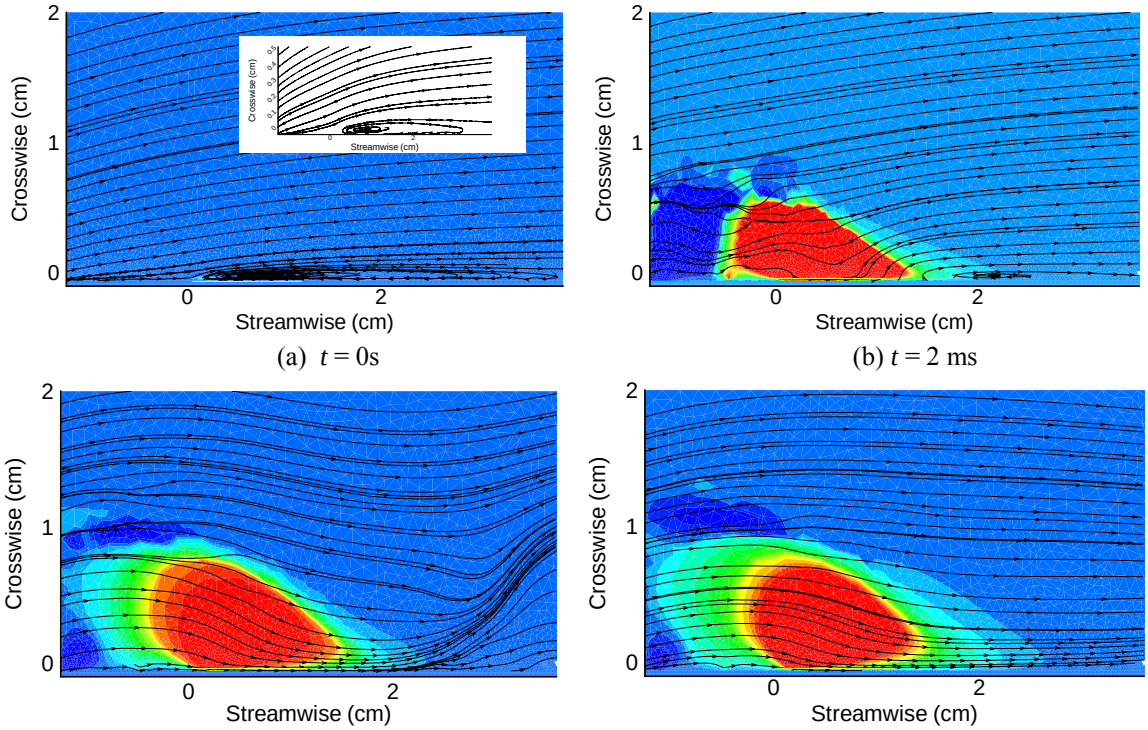

Figure 7. Separation control for an incoming flow with +12° AOA over a flat plate shows the gradual flow attachment eradicating the separation bubble in a few milliseconds. The velocity streamtraces are plotted over the streamwise specific force contours showing a strong average force over the exposed electrode.

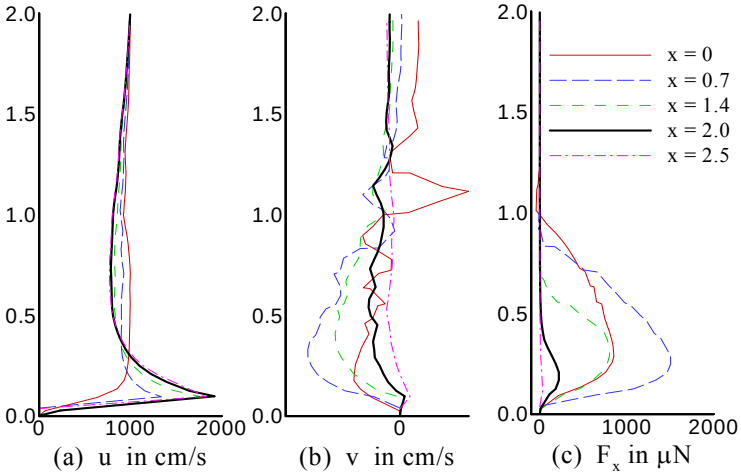

Figure 8. Velocity components and streamwise volume specific force distribution at specific locations (x in cm) normal to the dielectric surface after 6 ms.

VI. Conclusions

A two-dimensional finite element based formulation of plasma–fluid interactions is given for partially ionized plasma using the multi-component fluid equations. The model is applied to simulate an atmospheric surface dielectric barrier discharge for partially ionized helium gas. The computed results are similar to the experimental data showing that the exposed electrode is situated upstream of the peak location of the electric field and thus the imparted momentum. The two-dimensional predictions mimic the self-limiting discharge mechanism due to the charge accumulation on the insulator surface and the lowest electron current just beyond the peak applied voltage. Simulation results also show the effectiveness of plasma actuators for control of largely separated flows useful for many practical applications including airfoils and turbine blades. More investigation is needed to ascertain optimum electrochemical parameters. In our simulations, the electric field varies, but reaches a quasi-periodic asymptote. The electrode placement plays a significant role in controlling the separated flow. We believe the fluid reacts to the generated mean body force but may also weakly interacts as time evolves, however, this comment requires further clarification. In the near future, the model will be extended to air with negative ions and additional new mechanisms in the source terms. A model for realistic fully three-dimensional geometric and electrode configuration is also under development, as is an exploration of the effect of different voltage shapes (e.g. saw tooth, square wave etc.). The present effort thus provides a practical tool to augment experimental observations in exploring flow control concepts and in developing suitable inputs for traditional fluid dynamics codes based on the Navier-Stokes equations.

Acknowledgements

This work was partially supported by the Summer Faculty sponsorship of VAAC during the summer of 2004, the Air Force Research Laboratory contract no. F33615-98-D-3210, and AFOSR grants monitored by Dr. John Schmisseur. Authors acknowledge help from Dr. K.P. Singh and Mr. Haribalan Kumar for preparation of this paper.

References

[1]Corke, T. and Post, M., Proceedings of 43rd Aerospace Sciences Meeting, Reno, 2005 (AIAA, Washington, DC, 2002) Paper No. 2005-0563.
[2]C.L. Enloe, T.E. McLaughlin, R.D. VanDyken, K.D. Kachner, E.J. Jumper and T.C. Corke, *AIAA J., **42**, 595 (2004).*.
[3]J.R. Roth, Phys. Plasmas, **10**, 2117 (2003).
[4]W. Shyy, B. Jayaraman and A. Andersson, J. Appl. Phys., **92**, 6434 (2002).
[5]S. Roy and D. Gaitonde, J. Appl. Phys. **96**, 2476 (2004).
[6]S. Roy, Applied Physics Letters, **86** (10), 101502 (2005).
[7]S. Roy and D. Gaitonde, Proceedings of 43rd Aerospace Sciences Meeting, Reno, 2005 (AIAA, Washington, DC, 2002) Paper No. 2005-0160.
[8]Macheret, S. O., Shneider, M. N., and Miles, R. B., Journal of Propulsion and Power, **18**, 424 (2002).
[9]Shalaev, V., Fedorov, A., Malmuth, N., Zharov, V. and Shalaev, I., Proceedings of 41st Aerospace Sciences Meeting, Reno, 2003 (AIAA, Washington, DC, 2003) Paper No. 2003-0034.
[10]D. Gaitonde, Proceedings of 43rd Aerospace Sciences Meeting, Reno, 2005 (AIAA, Washington, DC, 2002) Paper No. 2005-0560.
[11]A. Bogaerts, E. Neyts, R. Gijbels and J. van der Mullen, Spectrochimica Acta Part B, **57**, 609 (2002).
[12]Gaitonde, D., Visbal, M. and Roy, S., AIAA Paper No. 2005-5302.
[13]K. Akhtar, J.E. Scharer, S.M. Tysk and E. Kho, Review of Scientific Instruments, **74**, 996 (2003).
[14]L. Ward, J. Appl. Phys. **33**, 2789 (1962).
[15]D. Balagangadhar and S. Roy, Computer Methods in Applied Mechanics and Engineering, **190**, 5465 (2001).
[16]S. Roy, B.P. Pandey, J. Poggie and D. Gaitonde, Physics of Plasmas, **10**, 2578 (2003).
[17]S. Roy and B.P. Pandey, Journal of Propulsion and Power, **19**, 964 (2003).
[18]S.M. Cooper, B.A. Cruden, M. Meyyappan, R. Raju and S. Roy, Nano Letters, **4,** 377 (2004).
[19]R. Raju and S. Roy, J. Thermophysics and Heat Transfer, **19**, 106 (2005).
[20]J.N. Reddy, An Introduction to the Finite Element Method, McGraw-Hill Book Company, New York, 1984.
[21]M. Riser, Comput. Methods Appl. Mech. Eng. **2**, 65 (1972).
[22]Jacob, J., Ramakumar, K., Anthony, R., and Rivir, R., *Fourth Int. Symp on Turbulence and Shear Flow Phenomena*, No. TSFP4-225, June 2005.
[23]F. Massines, A. Rabehi, P. Decomps, R.B. Gadri, P. Ségur and C. Mayoux, J. Appl. Phys., **83**, 2950 (1998).